Experimental Investigation of a New Hybrid Spar Buoy Wind Turbine With Oscillating Water Column

1st Beatrice Fenu
Department of Mechanical and Aerospace Engineering,
Polytechnic of Turin
Turin, Italy
beatrice.fenu@polito.it

2nd Mauro Bonfanti
Department of Mechanical and Aerospace Engineering,
Polytechnic of Turin
Turin, Italy
mauro.bonfanti@polito.it

3rd Mattia Glorioso
Department of Mechanical and Aerospace Engineering,
Polytechnic of Turin
Turin, Italy
mattia.glorioso@polito.it

4th Chiara Pilloton
Marine Technology Research Institute,
CNR-INM,
Rome, Italy
chiara.pilloton@inm.cnr.it

5th Andrea Bardazzi
Marine Technology Research Institute,
CNR-INM,
Rome, Italy
andrea.bardazzi@inm.cnr.it

6th Alessia Lucarelli
Marine Technology Research Institute,
CNR-INM,
Rome, Italy
alessia.lucarelli@inm.cnr.it

7rd Giovanni Bracco
Department of Mechanical and Aerospace Engineering,
Polytechnic of Turin
Turin, Italy
giovanni.bracco@polito.it

Abstract—Wave Energy Harvesters (WEH) struggle to be economically competitive in the energy market due to the high costs of installation with respect to the exploitable energy. The economic viability of WEHs could be enhanced through their integration into already existing floating platform, such as off-shore wind turbines. In this respect an experimental investigation of the hydrodynamic performances of a novel concept of hybrid platform is presented. The hybrid platform is composed of Oscillating Water Columns (OWC) integrated into a spar buoy floating wind turbine. The use of OWC represents a cost-effective solution to extend the operability of the system, increasing the annual working hours and stepping up the power extraction capability. This is obtained considering the delay between wind and wave energy exploitation. The experimental program is carried out in the CNR INM wave basin, based in Marine Technology Research Institute in Rome, Italy. Free decay and irregular wave tests are carried out to derive the dynamic behaviour of the new integrated energy harvester. Irregular sea states conditions are tested to reproduce the sea-environment in which the floating platform could be deployed. Particularly, the platform heave, roll, and pitch motion and the OWC pressures and water levels are analysed. The main outcome of this investigation regards the evaluation of the power production of the three OWCs installed on the floating platform and the influence of their geometric arrangement with respect to the wavefront.

Index Terms—Oscillating Water Column, Wind turbine, Hybrid platform, Experimental tests.

I. INTRODUCTION

Effective design, high economic efficiency and enhanced power capabilities, are essential stepping stones for reaching economic viability and industrial feasibility of offshore energy harvesters. Despite significant technological progress in recent years, especially in the field of wind energy, the target for a climate-neutral economy [1], [2] remains a distant prospect [3]. In the context of renewable energy, wave energy extraction still lacks standardized and economically efficient solutions. Despite the high energy content provided by ocean waves [4], a techno-economic feasibility analogous to existing technologies for wind energy conversion has not been achieved yet. In practice, a widespread solution to enhance the economic viability of Wave Energy Harversters (WEHs) could be their integration into already existing floating platform, such as offshore wind turbines [5], [6]. Moreover, floating wind turbines has the advantage that it can be used in high water depths where a further amount of energy can be harvested [7]. On the other hand, although significant progress has been made on WEHs

in the past few years, high costs are expected and slow down their commercialization [8].

Against this background, a new concept of floating hybrid platform is presented in this study: a multi-purpose wind-wave floating platform, composed of a wind turbine, installed on a spar buoy, surrounded by three Oscillating Water Colums (OWC). The choice to integrate the OWCs, despite other wave concepts, relies on the fact that this type of WEH can be directly connected to a floating platform and create a new rigid body. Higher stability and damped motion could be reached improving the wind turbine energy production. Moreover, the integration of OWCs into a wind turbine could reduce the economic impact of OWC installation by sharing the infrastructures, foundations, power electronics and cables with the already existing wind turbine. Motivated by this, Perez-Collazo et al. [9] developed a hybrid system for monopile substructures wind turbine, focusing on the integration with OWC and testing a scaled model experimentally. A new hybrid concept is presented by Cong et al. [10]. The study sees the integration on a monopile of a coaxial OWC and demonstrates that significant energy extraction efficiency is attained by the fluid motion inside the chamber and it is not restricted by wave direction. Cylindrical OWC are integrated in a monopile by Li et al. [11], finding an optimal wave condition to maximize the Capture Width Ratio (CWR). A tubolar structure ingrated OWC is presented by Zheng et al. [12] which presents a structural optimization towards improved power performance.

The aim of this paper is to investigate the hydrodynamics of the hybrid system and to evaluate the effect of the OWC on the motion of the floating platform. In addition, the power performance of the OWC are deepen to understand the energy feasibility of the hybrid system. The integration of OWC devices into already existing spar-buoy-type offshore wind turbine concepts remains untreated in literature.

The structure of this article follows. Section II briefly describe the hybrid platform proposed here, introducing its main dimensions in full-scale. Section III details the experimental setup, reporting the prototype dimensions and weights, sensors and acquisition system used, providing also technical designs and real snapshot of the physical prototype and the wave tank. Section IV presents the hydrodynamic analyses, reporting free-decay tests and hybrid platform motions in irregular wave, describing their effect on the OWCs vertical displacements. Section V analyses the OWC air pressure, water level and, at the end, the power production in irregular wave. Lastly, the main conclusion and achievement are discussed in Sect. VI.

II. FLOATING HYBRID PLATFORM

The hybrid platform proposed here is a new concept developed by the Marine Offshore Renewable Energy Lab (MOREnergy Lab[1]) of Politecnico di Torino (Italy). The design is carried out in accordance with the features of the installation site and the resource analysis of wind and wave resources. The chosen site is in the Mediterranean

[1] http://www.morenergylab.polito.it/

sea, precisely the Pantelleria island (Italy). The spar buoy platform and the WEH design were carried out to satisfy a trade-off between environmental constraints, mass properties and materials' costs. The spar buoy geometry is optimized accordingly to a techno-economic optimization of wind turbine platform for Mediterranean Sea [13]. The OWC dimensions has been estimated considering a cylindrical hollow shape for the design of the air chamber to ensures smoother air flow with respect to a squared-shape chamber [14]. The diameter of the air chamber is obtained by a linear relation to the wave parameters for the specific location. Accordingly to [15], to maximize the OWC power output, the characteristic parameter of the chamber can be estimated as follows:

$$d_{design} = 0.42\lambda_w \qquad (1)$$

where λ_w is the wavelength. Since the OWC device has to withstand the Mediterranean waves, the most occurring wavelength of the excitation waves is obtained from resource analysis and it is set equal to 47 [m]. The height of the camera is estimated following the consideration of Gomes et al. [16]. Three OWC are equally spaced around the circumference of the spar buoy with the aim to balance th platform and maximize the wave power extraction.

The Power Take Off (PTO) is represented by an impulse air turbine with an integrated generator for energy conversion. The size of the PTO represents critical design issue that affects the efficiency of the wave energy conversion system. The relationships between the geometrical parameters and the wave energy conversion efficiency is deepened in different studies [17], [18]. Here, the air turbine is modelled through an orifice on the top of the OWC chamber. The area-ratio of the orifice cross-section is the dimensionless ratio between the orifice area and the chamber waterplane area. This parameter is considered to control the influence on the performance of an OWC conversion system and it is defined as follows [19]:

$$R_o = A_o/A_c \qquad (2)$$

where A_o is the cross section-area of the orifice and A_c is the cross-section area of the air chamber.

The change in area ratio R_o directly influences the dynamic behaviour of the OWC, *i.e.* the air pressure and air flow inside it. The output power is expected to be larger with higher friction loss if the area ratio is large; on the other hand, a small orifice area produces less energy but less friction loss. The choice of the orifice directly influences the turbine duct area which in turn determines the turbine size. In operational condition characterized by wave period comparable to that one of Mediterranean Sea, it is recommended an orifice ratio smaller than $R_o < 2\%$ [17]. Therefore, the above-mentioned studies represent guidelines for the estimation of the optimal orifice ratio range in the case study, which in first hypothesis has been defined equal to 0.5%. A summary of the main dimensions of the OWC is presented in Tab. I.

TABLE I: Summary of the main size of OWCs' air chamber.

Quantity	Values
Diameter [m]	19.8
Height [m]	16.5
Angle between chambers [deg]	120
Areas ratio [%]	0.5

TABLE II: Summary of the main size of the hybrid platform prototype.

Quantity	Value
Spar Diameter [m]	0.35
Spar Height [m]	2.10
Platform draft [m]	1.86
OWC Diameter [m]	0.47
OWC Height [m]	0.39
OWC submerged height [m]	0.2
Tower Height [m]	2
Rotor diameter [m]	3
Total Weight [kg]	180
Mooring line length [m]	5.1
Mooring pre-tension [N]	10

III. EXPERIMENTAL SETUP

The experimental program was carried out in the wave basin of the National Council of Researches of Rome, Italy, with 220 [m] long, 9 [m] wide, 3.8 [m] deep. A unidirectional wave maker is installed on one side of the wave basin and face up the dissipative beach on the other side.

The Fixed Reference Axis (FRA), named XYZ, is oriented in the way the X-axis run along the length of the wave tank, the Y-axis run on the width of the wave tank and the Z-axis pointed outwards. Its origin is located where the prototype was installed in correspondence of the water free surface. Froude similarity [20] was used to scale down the model with a geometrical scale of $\lambda = 1/42$. The scale was selected as a trade off between the dimensions of the facility and the best experiments quality by minimizing the scale effect.

A. Prototype design

The model is a complex system formed by several elements and shown in Fig. 1a. The substructure is made of aluminum. It is composed by a vertical 2.1 m long cylinder that represents the spar, and three small cylinders that represent the air chambers of the OWCs. The ballast is made of lead disks and it is located at the bottom of the vertical body. The OWC chamber top plates included a central opening to test different PTO damping conditions. The nonlinear/quadratic pressure–flow rate induced by the PTO system is simulated during experiments using an orifice to simulate an impulse turbine. The orifice diameter is adapted by 3D printer plugs and used to model nonlinear PTO damping. The wind turbine is located on the top of the spar thanks to a 3D printed coupling element. It is composed by the tower made in PVC, mechanical parts to form the rotor and three blades made in foam. The overall weight of the model, including the ballast weights, as well as the sensors installed inside the chambers was around 180.00 [kg]. The mooring system consists in three lines symmetrically arranged. Each line is composed by a non-elastic rope, followed by a spring, that is connected to a load cell thanks to a cable rod. The rope is attached to the fair-leads on the spar and pre-tensioned on an horizontal plane by the cable rod of 10 N. The lines are spaced with an angle of 120°, two lines front wave and one line on the back of the model. This type of mooring configuration was used to represent the theoretic stiffness matrix applied to the model. A geometrical scaling procedure of the mooring system was ruled out due to the dimension limits of the facility.

In Tab. II the main dimension of the prototype are summarized.

B. Sensors and acquisition system

In the experiments, each subsystem is studied with different sensors. The sensors are listed from the top of the wind turbine downwards. A motion tracking system (Krypton) is used to measure the motion of the whole platform with respect the FRA system, and its markers are installed on the wind turbine tower and redundant with an inertial measurement unit (MTi-100 Xsens). Each of the air chambers have installed on the top one Ultrasonic water level sensors (Autosen AU011) to measure the instantaneous free surface elevation inside the chamber, and two differential pressure sensors (Amphenol 001PD ELVH serie). The Ultrasonic sensor was located 10 cm from the wall of the OWC chamber, while the pressure sensors were located in mirror position with respect the wave front direction. The mooring system was instrumented with three load cell, one for each line, to quantify the loads acting on the lines. In addition two wave gauges were installed between the wave maker and the model to verify the wave propagation along the wave tank.

The goals of the physical measurement were to study the effect of the incoming wave on the hydrodynamic performance of the floating structure and on the thermodynamic of the air chamber. In Section IV the analysis performed are investigated.

IV. HYDRODYNAMIC ANALYSIS

In this section, the hydrodynamic behaviour of the hybrid platform is analyzed, focusing on its vertical (heave) and angular (roll and pitch) motion. The kinematic of the structure is evaluated performing free decay tests and test under irregular waves. The former aims to identify the natural frequencies of the hybrid platform, while the latter aims to show the effect of the structure motion on the vertical displacement of the OWC chambers and their power performance.

A. Free decay tests

Before addressing the main purpose of the work, it is useful to analyze the behaviour of the hybrid platform with free decay tests to find its natural frequency in different Degree of Freedom (DoF). The free decay tests are performed for Heave, Roll and Pitch DoF. Each test was performed by forcing an initial displacement of the structure for a single DoF at a time and then released until the oscillations were exhausted. The repeatability of the test is verified performing the tests several

(a) Schematic of the hybrid platform and its main components

(b) A photograph of the physical device deployed in the towing tank

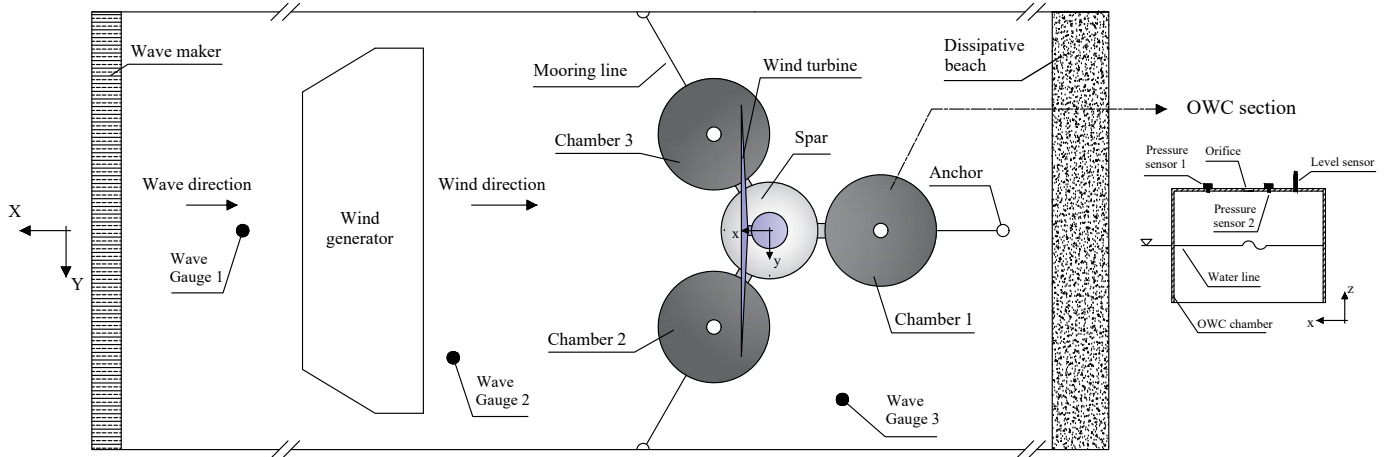Fig. 1: **(a) Schematic representation and (b) photograph of the hybrid platform**.

Fig. 2: Schematic representation of the experimental setup: the wave tank, the hybrid platform and a lateral section of the OWC chamber with sensors installed inside.

times and the uncertaties analysis is performed. The results are shown in Fig. 3 and present the resonant periods tested with a relative error between the measurement and the average value of maximum 3% for heave motion, 1% for roll motion and 2% for pitch motion.

Fig. 3 shows the adimensional free oscillation of the model for Heave, Roll and Pitch. It can be noticed that the angular motions present similar resonant frequencies, while the heave motion presents a higher resonant frequency and short extinguish of the oscillation. This behaviour is due to the strong influence of the non-linear orifice damping of the OWCs on the hydrodynamic of the floater. The resonant frequencies and the

motion of the device are summarized in Table III and shown in Figure 3.

TABLE III: Natural frequencies of the structure obtained from the free decay tests.

DoF	Symbol	Value [Hz]
Heave	f_z	0.602
Roll	f_α	0.127
Pitch	f_δ	0.129

B. Irregular wave test

For the upcoming experimental tests, irregular wave input are generated considering a Jonswap parametric form [21]. The
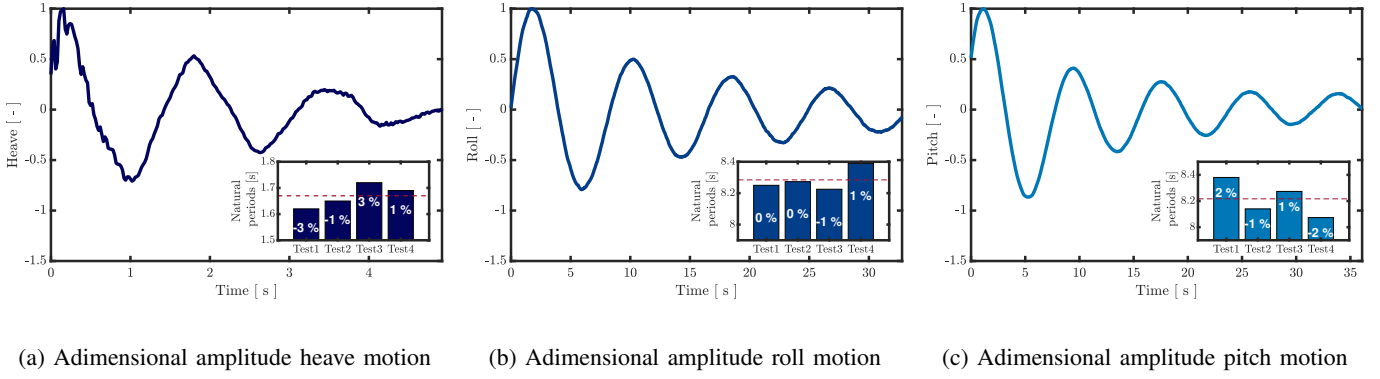
(a) Adimensional amplitude heave motion   (b) Adimensional amplitude roll motion   (c) Adimensional amplitude pitch motion

Fig. 3: **(a)** Heave, **(b)** roll and **(c)** pitch motion amplitudes induced by the free decay tests.

Spectral Density Function (SDF) of a Jonswap spectrum can be written as a function of several parameters: γ, defined as the peak enhancement factor, H_s, named the significant wave height, and f_p, the peak frequency. In this work, a Jonswap spectrum characterised by a peak enhancement factor γ=3.3, a significant wave height H_s=5.2 [cm], and a peak frequency f_p=0.86 [Hz] has been chosen to be representative of a realistic working condition for the model scale. According to the wave superposition method known as Harmonic Deterministic Amplitude (HDA) [22], a so-called wave realisation η can be generated by discretizing a generic Jonswap spectrum $S_{\eta\eta}$ in $M + 1$ frequencies $f_w = w\Delta f$, $\forall w \in \{0, ..., M\}$, with a frequency step $\Delta f = 1/T_{sim}$, with T_{sim} as the corresponding duration of one single experiment, set to T_{sim}=500 [s]. It can be noticed that T_{sim} is chosen to be sufficiently large to obtain statistically consistent results for the upcoming performance assessment [22]. Then, the wave signal $\eta(X, t)$ can be generated at a specific longitudinal position X on the towing tank as:

$$\eta(X, t) = \sum_{w=0}^{M} \eta_{0w} \cos(k_w X - 2\pi f_w t + \phi_w) \qquad (3)$$

where k_w is the wave number, ϕ_w are the phases randomly chosen following a uniform distribution in $[0, 2\pi]$, and $\eta_{0w} = \sqrt{2 S_{\eta\eta}(f_w)\Delta f}$. The wave maker generates a random wave profile η underling a Jonswap spectrum with a specific random seed verified by preliminary tests carried out in the absebce of the prototype and by replacing it with a wave probe, located specifically at X position.

To begin with the corresponding performance assessment, Fig. 4 superposes the wave amplitudes ($\overline{\eta}$) obtained via Fast Fourier Transform (FFT) of the signal captured by the undisturbed wave gauge (WG1) and the amplitudes of Heave ($\overline{z}$), Roll ($\overline{\alpha}$) and Pitch ($\overline{\delta}$) motion of the hybrid platform.

The FFTs of the motions have been placed in the right-hand axis to be able to compare them with the FFT of the wave signal. Concerning the heave motion, Fig. 4a highlights that the platform exhibits several distinct peaks: one is centred at the wave peak frequency f_p, and many others toward the heave resonance period f_z. A JONSWAP spectrum excites a
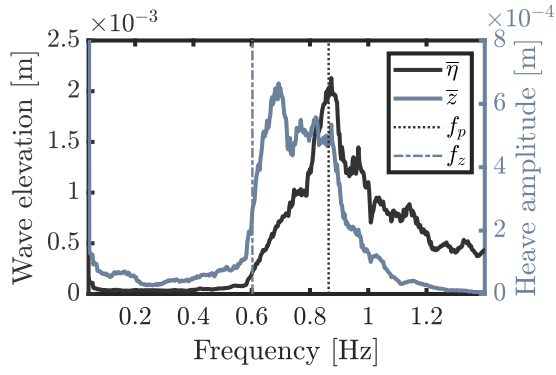
precise frequency band, mainly depending on the chosen peak enhancement factor. Although the energy of the spectrum is concentrated around its peak frequency f_p, the platform also exhibits a marked oscillation around its heave resonance frequency, f_z, of greater amplitude than the oscillation at the wave frequency. This behaviour is more evident for Roll and Pitch DoF, reported in Fig. 4b and Fig. 4c, respectively. Here, the distinction between the motion generated by the frequency content of the input wave and the motion in correspondence with the natural frequency of the angular DoFs is even sharper. The most striking result that emerges from the data analysis is that the angular motion generated from the natural oscillation of the platform is larger than the one forced by the input wave. This is not evident for the heave DoF since the natural frequency of the heave DoF is quite close to the wave excitation frequency and, therefore, the resonance and wave-induced effects cannot be distinguished. This is not the case for the other two DoFs (roll and pitch) as their natural frequencies are about an order of magnitude smaller that the input wave. It is also worth noting that the magnitude of the roll motion is one order of magnitude lower than the pitch one, due to the fact that the wave generated is unidirectional and directed along the X direction (as reported in Fig. 1).

To deeply understand the influence of the angular motion of the platform on the vertical motion of the OWC chambers, it is possible to calculate the vertical motion induced at the chambers as the sum of three contributions: pure heave motion, roll-induced vertical motion, and pitch-induced vertical motion. Since the OWC chambers are eccentric with respect to the centre of gravity of the structure in both the X- and Y-direction, their absolute vertical motion can be computed as:
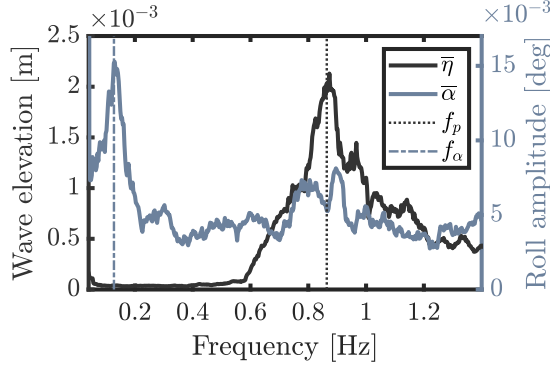
$$z_1 = z + r\sin(\psi)\sin(\alpha) + r\cos(\psi)\sin(\delta) \qquad (4a)$$

$$z_2 = z - r\cos\left(\frac{\pi}{6} - \psi\right)\sin(\alpha) - r\cos\left(\frac{\pi}{3} + \psi\right)\sin(\delta) \quad (4b)$$
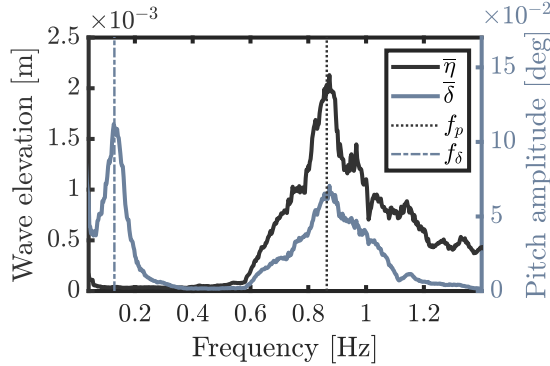
$$z_3 = z + r\cos\left(\frac{\pi}{6} + \psi\right)\sin(\alpha) - r\cos\left(\frac{\pi}{3} - \psi\right)\sin(\delta) \quad (4c)$$

(a) Amplitudes of wave and heave motion.

(b) Amplitudes of wave and roll motion.

(c) Amplitudes of wave and pitch motion.

Fig. 4: Wave amplitudes superposed to **(a)** heave, **(b)** roll and **(c)** pitch motion amplitudes.

where r is the radial distance between the vertical centre of the floating platform and the center of the OWC chamber, measured on the horizontal plane of the platform reference system (xy). The first terms in the Eq. 4 refers to pure heave motion of the whole platform. The second terms in the sum refers to the vertical motion of the chambers induced by the rolling oscillation. As can be seen, in the absence of yaw motion, the chamber behind the wave front (chamber 1) would not experience any roll-induced vertical motion. The other two chambers (chamber 2 and chamber 3), are eccentric to the y-axis of the platform and are therefore affected by the roll motion. Concerning the pitch motion contribution, chamber 1

is at maximum eccentricity in x direction, equal to r, minus the reduction due to the cosine of the yaw angle ψ. The other two chambers (chamber 2 and chamber 3) also undergo a vertical motion generated by the pitch oscillation, although to a lesser extent than chamber 1 since they have an inclination of $\pi/3$ with respect to the x-axis of the platform. The analytical derivation of the Eq. 4 for a rigid body is straightforward and the reader should refer to [23] for a clearer understanding. Motivated by this, we superpose, in Fig. 5, the FFT of four different signals releated to each OWC chamber: the heave motion z, with a continuous grey line, the roll-induced vertical motion ($z_{\alpha,1}$, $z_{\alpha,2}$, and $z_{\alpha,3}$), with a light coloured continuous line, the pitch-induced vertical motion ($z_{\delta,1}$, $z_{\delta,2}$, and $z_{\delta,3}$), with a dark coloured continuous line, and the whole vertical motion (z_1, z_2, and z_3), with a black dot-dashed line. The subscripts 1, 2, and 3 refer to chamber 1, chamber 2 and chamber 3, respectively.

Firstly, it is shown how, especially for chamber 1 (see Fig. 5a), the vertical motion induced by the pitch oscillation is of the same order of magnitude of the heave motion alone, and for specific frequency ranges even higher. In particular, a clear low-frequency peak results for all three chambers, induced by the low-frequency components of roll and pitch motion, although those relating to the latter are reasonably more pronounced. The differences between chamber 2 and chamber 3 (see Fig. 5b and Fig. 5c), which are theoretically symmetrical about the X-axis of the tank, are due to an offset in the yaw degree of freedom. As shown in Fig. 6, reporting a time trace of the yaw motion, the platform is slightly oriented at a yaw angle almost equal to 5.5 degrees. This slight asymmetry could be caused by the assessment of pre-loads assigned to the mooring lines combined with a slight constructive asymmetry of the platform. For that reason, the arm along the roll DoF is larger than the arm along the pitch DoF. Concerning the whole vertical motion of the chambers, Fig. 5 reveals two opposing behaviours in the frequency range of the generated wave: for chamber 1, the pitch-induced ($z_{\delta,1}$) and heave vertical (z) motions create destructive interference, generating a vertical motion of the chamber (z_1) that is smaller than both contributions; on the other hand, in chamber 2 and 3, the pitch-induced motions ($z_{\delta,2}$ and $z_{\delta,3}$) favours an increase in the vertical displacements and thus the FFTs of z_2 and z_3 are larger than the FFTs of the individual contributions.

C. Principal remarks

The most important finding is how the angular motions of the platform on the vertical motions of the OWCs can affect their productivity. Furthermore, it is recalled that the platform presents a vertical symmetry (xz plan) at the midpoint of each of the OWCs and, as a consequence, the platform will have a certain degree of independence from the wave direction as its hydrodynamic behaviour is repeatable at an angle of 60 [deg], as shown in Fig. 7. The sky-blue region represents the set of wave directions in which the platform behaves differently, as the orientation of the wave front changes. The advantage is the multi-directionality of the wave converters, approaching to the
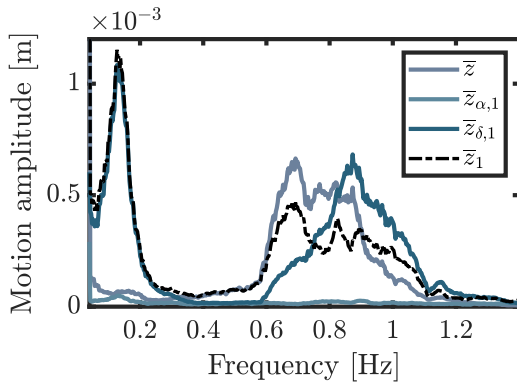
(a) Amplitudes of heave motion, roll-induced motion, and pitch-induced motion, and total vertical motion for chamber 1. .
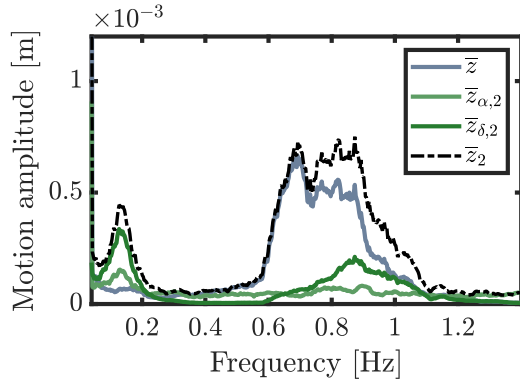
(b) Amplitudes of heave motion, roll-induced motion, pitch-induced motion, and total vertical motion for chamber 2.
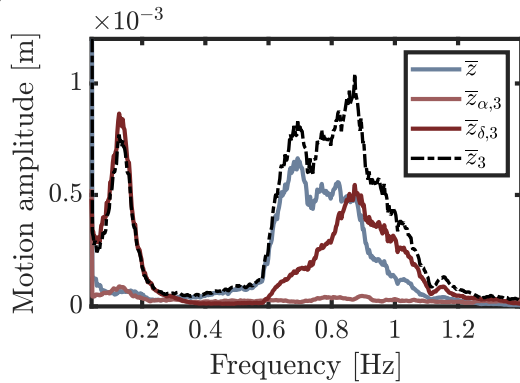
(c) Amplitudes of heave motion, roll-induced motion, pitch-induced motion, and total vertical motion for chamber 3.

Fig. 5: Vertical motion amplitudes of the OWC chambers, obtained by a pure heave motion, a roll-induced motion, and a pitch-induced motion. **(a)** chamber 1, **(b)** chamber 2, and **(c)** chamber 3.

functioning in a real environment. In addition, the distance r of the chambers from the geometric centre of the spar influences the dynamics of the OWCs and the hydrostatic stiffness of the entire structure. The influence of the number of chambers and their radial and circumferential arrangement around the spar will be the subject of numerical and experimental studies
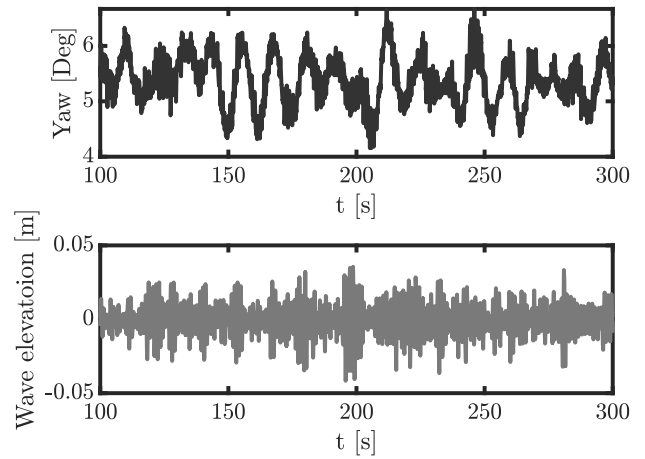

Fig. 6: Time series of the yaw motion (ψ) of the hybrid platform in irregular wave conditions and the corresponding wave elevation.

in future work with the aim of maximize the OWC power production and minimize the vertical and angular oscillations of the wind turbine.
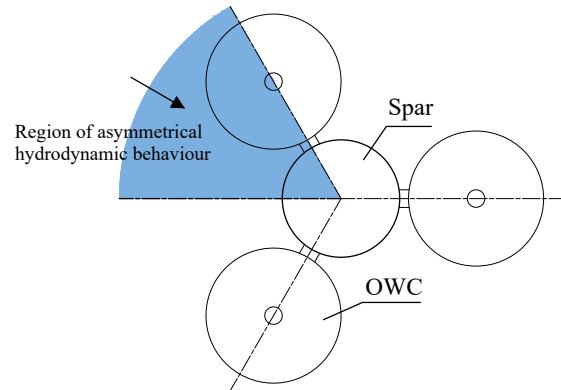

Fig. 7: Schematic representation of wave directions in which the hydrodynamic behaviour of the platform is sensitive to the wave direction encountered.

V. OWC PERFORMANCES

In this section, the dynamic behaviour and the power production of the OWCs are analysed. In particular, for each chamber the pressure, water level and its time derivative were analysed by FFT and time series to highlight the frequency content and phase relationship to calculate the pneumatic power produced by the OWCs.

A. Water level and pressure inside the chambers

A quantitative description of the relative motion of water inside the OWC chamber is provided in Fig. 8, where the water level amplitudes are superposed to the vertical displacement amplitudes of each OWCs chamber. The comparison of the water level amplitudes (h_1, h_2 and h_3) shows the difference in oscillation between front wave chambers (chamber 2 and

chamber 3) and backward one (chamber 1). For the latter, the vertical motion induced by the pitch creates destructive interference, decreasing the relative motion of the water inside the chamber. On the contrary the vertical motion of the frontal chambers is amplified by pitch motion, creating a constructive interference. It can be seen from Fig. 8 that the relative level within the chambers mimics the vertical motion of the chambers themselves, except for a small discrepancy in absolute value, caused by the fact that the relative level h is a function of the vertical motion of the platform, and also of the vertical motion of the water column within the chambers. This suggests that the relative water level inside the OWC is remarkably influenced not only from the hydrodynamic behaviour of the water columns but also from the motion of the floating structure. This confirm the remark assessed at the end of Sect. IV, stating that the geometric layout of the OWC is an important design parameter for the proposed hybrid platform.
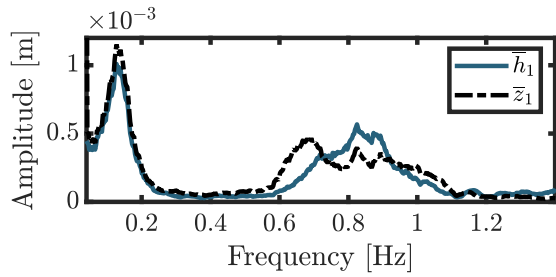
(a) Amplitudes of water level and total vertical motion of chamber 1.
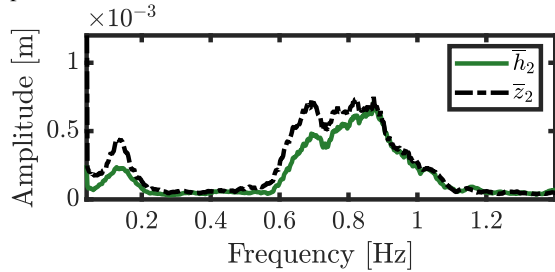
(b) Amplitudes of water level and total vertical motion of chamber 2.
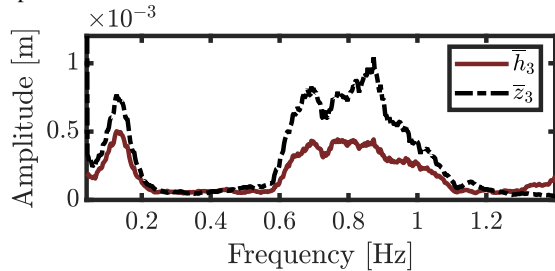
(c) Amplitudes of water level and total vertical motion of chamber 3.

Fig. 8: Relative water level and total vertical motion amplitudes of the OWC chambers. **(a)** chamber 1, **(b)** chamber 2, and **(c)** chamber 3.

Concerning the pressure variation, reported in Fig. 9, it is shown how the chamber 1 is considerably disadvantaged compared to the others, as expected. Here, the pressure levels

are about three times lower than in chamber 2 and 3. On the other side, chamber 2 and 3 present similar pressure variation. The expected results should follow the same trend of water level variation. Despite the differences in term of water level h_2 and h_3, captured in Fig. 8b and Fig. 8c, it is worth mentioning that fluid height is measured with ultrasonic sensors that give average measurements. In fact, pressure dynamics are also influenced by sloshing motions within the chamber that inevitably influence the pressure distribution and cause discrepancies between water level and pressure trends. Future studies will aim to analyse in depth also the dynamics inside the chambers so that, for example, the influence on the energy extraction of radial size of OWC in relation to the period of the incident wave. Finally, it should be noted that the low-frequency pressure peak caused by the pitch and roll motions is about one order of magnitude smaller than that at the wave frequency, suggesting that the motion induced by the angular oscillations will not contribute significantly to the OWC's energy production at low frequencies.
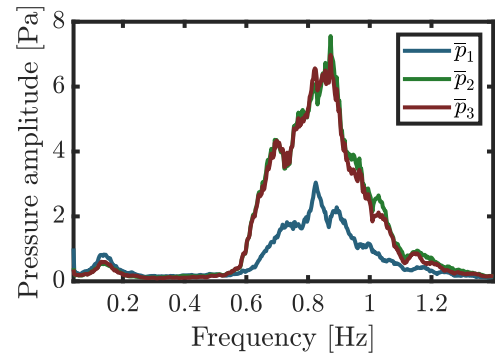

Fig. 9: Chamber pressure amplitues.

B. Power production

The average pneumatic power produced from the three air chambers is computed with the purpose of calculate the performance of this new type of hybrid platform. The average power absorbed can be calculated from the measured air pressure p and air volume flux q, as follows:

$$\overline{P} = \frac{1}{T_{sim}} \int_0^{T_{sim}} P(t)\, dt =$$
$$= \frac{1}{T_{sim}} \int_0^{T_{sim}} p(t)q(t)\, dt = \frac{1}{T} \int_0^{T_{sim}} p(t)\dot{h}(t)A_w\, dt \quad (5)$$

where A_w is the cross-sectional area of the free surface inside the chamber, p the air pressure, and $\dot{h}$ is the time rate of change of the water level h. $\dot{h}$ is calculated by a third-order approximation of the first time derivative of h [24], as follows:

$$\dot{h} = \frac{-11h(t) + 18h(t+\Delta t) - 9h(t+2\Delta t) + 2h(t+3\Delta t)}{6\Delta t} \quad (6)$$

where Δt is the time step between two consecutive data points. The extracted power is computed for all the duration of the

wave test, equal to T_{sim}=500 [s]. Equation 5 represents the power input to an OWC system, and its mean value can be assumed to be equal to the power that would be obtained by using the orifice flow rate if the losses due to friction through the air orifice are ignored [25].

The average power produced from each OWC is reported in Tab. IV. As expected, the power extracted from the two frontward chambers (chamber 2 and chamber 3) is larger than the one extracted from the chamber behind the wave front (chamber 1). Predictably, since the water level h fluctuates more in chamber 2 (as shown in Fig. 5 the Fig. 8) and that the pressure distributions within the chambers are almost equivalent (as reported in Fig. 9), chamber 2 produces about 25% more than chamber 3, unless there is a slight asymmetry due to a tilt angle around the vertical axis of the turbine (as demonstrated in Fig. 7).

Fig. 10: Time series of the OWC power ($P(t)$) in irregular wave conditions for chamber 2 and chamber 3.

TABLE IV: Power production of OWC chambers.

Chamber Id	Symbol	Value [W]
1	$\overline{P}_1$	-0.031
2	$\overline{P}_2$	-0.136
3	$\overline{P}_3$	-0.105

Fig. 10 reports the time histories of instantaneous power $P(t)$ of chamber 2 and chamber 3. Looking at the right box in Fig. 10, it is evident that the average power extracted from chamber 2 is higher because the time rate of change of the water level h_2 is higher in respect to the h_3 one. Furthermore, assuming the power extracted from the OWC to be negative in Fig. 10, it can be seen that a contribution of reactive power appears, i.e. power with a positive sign. In this work, the power extracted at the orifice is not directly calculated, since the actual flow disposed of by the orifice is not measured. Then, the time trace of the instantaneous pneumatic power, computed multiplying the time traces of $p(t)$ and $q(t)$, has a share of reactive power due to the spring-like effect of the air chamber. If the flow disposed by the orifice were used, the instantaneous power would have no reactive component, since the orifice system is purely passive. However, the reactive power is very small compared to the active one, and it allows to conclude that the time series of the power at the outlet of the OWC orifice will be almost equal to the time series of the power at the chamber inlet. This lead to the assumption that the air can be treated as in-compressible fluid in small scale OWCs, as verified [26].

VI. Conclusion

The present experimental investigation is designed to establish a proof-of-concept of a novel hybrid Wind-Wave energy converter. The device includes a spar-buoy wind turbine surrounded by three OWC chambers that convert the energy of the incident waves to pneumatic power. A preliminary experimental investigation is carried out to study the hydrodynamic performance of the platform with free decay and irregular wave tests.

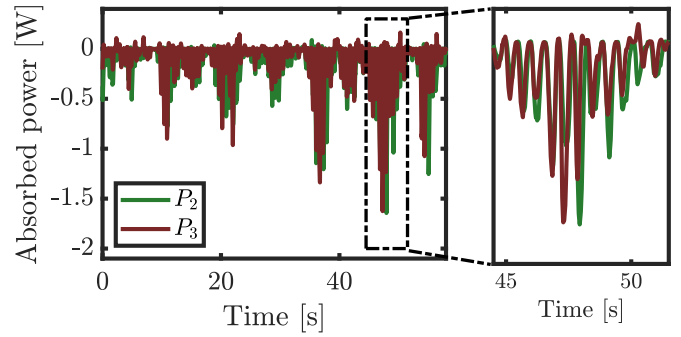The results of this investigation indicate that this configuration has the potential to use OWC-type WEHs to both stabilize floating wind turbines and produce electrical power. The experimental tests, albeit preliminary, indicates that the angular motions of the platform influence the hydrodynamic behaviour of the OWC chambers. Although it was taken for granted that the oscillating motion of the platform contributed to some extent to the vertical motion of the chambers, it was shown that this motion is of the same order of magnitude as the heave displacement of the platform alone and further studies will assess if it contributes positively or not to the energy generation of OWCs. Moreover, it was found that the mutual interaction between the three chambers has a relevant impact on increasing or decreasing the power extracted from the OWC, depending on the direction of the wave front relative to the platform. As expected, the OWC chamber located backward to the wave front, has the lower productivity, while the forward chambers the highest. In particular, the two chambers in front of the platform, show quite different productivity, caused by the different volumetric flow rate generated inside the chamber. This different behaviour will be the subject of further numerical and experimental studies.

The present experimental work will be expanded considering both regular and irregular seas, different orifice dimensions and regular wind conditions to assess the reciprocal influence of wind-wave interaction on platform hydrodynamic and OWC power extraction performances. In further experiments the setup will be carried out avoiding asymmetrical position of the floater. Furthermore, the experimental results will be used as a bench-marking validation for the hybrid platform numerical model.

References

[1] D. Connolly, H. Lund, and B. V. Mathiesen, "Smart Energy Europe: The technical and economic impact of one potential 100% renewable energy scenario for the European Union," Renewable and Sustainable Energy Reviews, vol. 60, pp. 1634–1653, 2016.

[2] EU, "Clean Energy for all Europeans Package, The Clean Energy Package – CEP," pp. 2018–2020, 2020. [Online]. Available: https://ec.europa.eu/energy/topics

[3] ——, "Directive (EU) 2018/2001 of the European Parliament and of the Council of 11 December 2018 on the promotion of the use of energy from renewable sources," pp. 82–209, 2018. [Online]. Available: https://eur-lex.europa.eu/

[4] M. Melikoglu, "Current status and future of ocean energy sources: A global review," Ocean Engineering, vol. 148, no. November 2017, pp. 563–573, 2018. [Online]. Available: https://doi.org/10.1016/j.oceaneng.2017.11.045

[5] E. Petracca, E. Faraggiana, A. Ghigo, M. Sirigu, G. Bracco, and G. Mattiazzo, "Design and Techno-Economic Analysis of a Novel Hybrid Offshore Wind and Wave Energy System," Energies, vol. 15, no. 8, 2022. [Online]. Available: https://www.mdpi.com/1996-1073/15/8/2739

[6] B. Fenu, V. Attanasio, P. Casalone, R. Novo, G. Cervelli, M. Bonfanti, S. Sirigu, G. Bracco, and G. Mattiazzo, "Analysis of a Gyroscopic-Stabilized Floating Offshore Hybrid Wind-Wave Platform," Journal of Marine Science and Engineering, jun 2020. [Online]. Available: https://www.mdpi.com/2077-1312/8/6/439

[7] M. Karimirad, Offshore Energy Structures: For Wind Power, Wave Energy and Hybrid Marine Platforms. Springer, 2014.

[8] M. Mustapa, O. Yaakob, Y. M. Ahmed, C.-K. Rheem, K. Koh, and F. A. Adnan, "Wave energy device and breakwater integration: A review," Renewable and Sustainable Energy Reviews, vol. 77, pp. 43–58, 2017. [Online]. Available: https://www.sciencedirect.com/science/article/pii/S1364032117304409

[9] C. Perez-Collazo, R. Pemberton, D. Greaves, and G. Iglesias, "Monopile-mounted wave energy converter for a hybrid wind-wave system," Energy Conversion and Management, vol. 199, p. 111971, 2019. [Online]. Available: https://www.sciencedirect.com/science/article/pii/S019689041930977X

[10] P. Cong, B. Teng, W. Bai, D. Ning, and Y. Liu, "Wave power absorption by an oscillating water column (owc) device of annular cross-section in a combined wind-wave energy system," Applied Ocean Research, vol. 107, p. 102499, 2021. [Online]. Available: https://www.sciencedirect.com/science/article/pii/S0141118720310580

[11] Y. Li, S. Liu, C. Xu, D. Li, and H. Shi, "Experimental study on the cylindrical oscillating water column device," Ocean Engineering, vol. 246, p. 110523, 2022. [Online]. Available: https://www.sciencedirect.com/science/article/pii/S0029801822000038

[12] S. Zheng, G. Zhu, D. Simmonds, D. Greaves, and G. Iglesias, "Wave power extraction from a tubular structure integrated oscillating water column," Renewable Energy, vol. 150, pp. 342–355, 2020. [Online]. Available: https://www.sciencedirect.com/science/article/pii/S0960148120300094

[13] A. Ghigo, L. Cottura, R. Caradonna, G. Bracco, and G. Mattiazzo, "Platform optimization and cost analysis in a floating offshore wind farm," Journal of Marine Science and Engineering, vol. 8, no. 11, 2020. [Online]. Available: https://www.mdpi.com/2077-1312/8/11/835

[14] S. S. Abbasi, T. H. Min, S. H. Shafiai, S. Y. Theng, and L. Heng, "Design enhancement of an oscillating water column for harnessing of wave energy," 2017.

[15] M. Sameti and E. Farahi, "Output Power for an Oscillating Water Column Wave Energy Converter," Ocean and Environmental Fluid Research, vol. 1, no. 2013, pp. 2331–5105, 2014.

[16] M. N. Gomes, C. D. Nascimento, B. L. Bonafini, E. D. Santos, L. A. Isoldi, and L. A. O. Rocha, "Two-Dimensional Geometric Optimization of an Oscillating Water Column Converter in Laboratory Scale," Revista de Engenharia Térmica, vol. 11, no. 1-2, p. 30, 2012.

[17] D. Z. Ning, R. Q. Wang, Q. P. Zou, and B. Teng, "An experimental investigation of hydrodynamics of a fixed OWC Wave Energy Converter," Applied Energy, vol. 168, pp. 636–648, 2016. [Online]. Available: http://dx.doi.org/10.1016/j.apenergy.2016.01.107

[18] H. H. Lee and C. H. Chen, "Parametric study for an oscillating water column wave energy conversion system installed on a breakwater," Energies, vol. 13, no. 8, 2020.

[19] M. Shalby, P. Walker, and D. Dorrell, The investigation of a segment multi-chamber oscillating water column in physical scale model, 2016.

[20] R. G. Coe and V. S. Neary, "Review of methods for modeling wave energy converter survival in extreme sea states," Proceedings of the 2nd Marine Energy Technology Symposium (METS2014), no. April, pp. 1–8, 2014.

[21] K. Hasselmann, T. P. Barnett, E. Bouws, H. Carlson, D. E. Cartwright, K. Eake, J. A. Euring, A. Gicnapp, D. E. Hasselmann, P. Kruseman, A. Meerburg, P. Mullen, D. J. Olbers, K. Richren, W. Sell, and H. Walden, "Measurements of wind-wave growth and swell decay during the joint North Sea wave project (JONSWAP)." Deut. Hydrogr. Z., vol. 8, pp. 1–95, 1973.

[22] A. Merigaud and J. V. Ringwood, "Free-Surface Time-Series Generation for Wave Energy Applications," IEEE Journal of Oceanic Engineering, vol. 43, no. 1, pp. 19–35, 2018.

[23] T. Perez, Ship Motion Control: Course Keeping and Roll Stabilisation Using Rudder and Fins. Springer London, 2005.

[24] K. Rezanejad, J. F. M. Gadelho, S. Xu, and C. G. Soares, "Experimental investigation on the hydrodynamic performance of a new type floating Oscillating Water Column device with dual-chambers," Ocean Engineering, vol. 234, p. 109307, 2021. [Online]. Available: https://www.sciencedirect.com/science/article/pii/S0029801821007253

[25] D.-z. Ning, Y. Zhou, R. Mayon, and L. Johanning, "Experimental investigation on the hydrodynamic performance of a cylindrical dual-chamber Oscillating Water Column device," Applied Energy, vol. 260, p. 114252, 2020. [Online]. Available: https://www.sciencedirect.com/science/article/pii/S0306261919319397

[26] A. Elhanafi, G. Macfarlane, A. Fleming, and Z. Leong, "Scaling and air compressibility effects on a three-dimensional offshore stationary OWC wave energy converter," Applied Energy, vol. 189, pp. 1–20, 2017. [Online]. Available: https://www.sciencedirect.com/science/article/pii/S0306261916317263